

# Relative intensity noise and intrinsic properties of RF mounted interband cascade laser

Cite as: Appl. Phys. Lett. **119**, 171107 (2021); <https://doi.org/10.1063/5.0070981>

Submitted: 10 September 2021 • Accepted: 05 October 2021 • Published Online: 26 October 2021

 P. Didier,  O. Spitz,  L. Cerutti, et al.



View Online



Export Citation



CrossMark

## ARTICLES YOU MAY BE INTERESTED IN

**Threshold behavior in spin lasers: Spontaneous emission and nonlinear gain**  
 Applied Physics Letters **119**, 171104 (2021); <https://doi.org/10.1063/5.0069125>

**Charge-density-wave quantum materials and devices—New developments and future prospects**  
 Applied Physics Letters **119**, 170401 (2021); <https://doi.org/10.1063/5.0074613>

**Structural stability of open vortex beams**  
 Applied Physics Letters **119**, 171105 (2021); <https://doi.org/10.1063/5.0062967>



1 qubit

Shorten Setup Time  
**Auto-Calibration**  
**More Qubits**

Fully-integrated  
**Quantum Control Stacks**  
**Ultrastable DC to 18.5 GHz**  
 Synchronized <<1 ns  
 Ultralow noise



100s qubits

[visit our website >](#)



# Relative intensity noise and intrinsic properties of RF mounted interband cascade laser

Cite as: Appl. Phys. Lett. **119**, 171107 (2021); doi: [10.1063/5.0070981](https://doi.org/10.1063/5.0070981)

Submitted: 10 September 2021 · Accepted: 5 October 2021 ·

Published Online: 26 October 2021



View Online



Export Citation



CrossMark

P. Didier,<sup>1,2,a)</sup>  O. Spitz,<sup>1</sup>  L. Cerutti,<sup>3</sup>  D. A. Diaz-Thomas,<sup>3</sup>  A. N. Baranov,<sup>3</sup>  M. Carras,<sup>2</sup> and F. Grillot<sup>1,4</sup> 

## AFFILIATIONS

<sup>1</sup>LTCI Télécom Paris, Institut Polytechnique de Paris, 19 Place Marguerite Perey, Palaiseau 91120, France

<sup>2</sup>mirSense, Centre d'intégration Nanolnnov, 8 Avenue de la Vauve, Palaiseau 91120, France

<sup>3</sup>Institut d'Electronique et des Systèmes, Université de Montpellier, CNRS UMR 5214, Montpellier 34000, France

<sup>4</sup>Center for High Technology Materials, University of New-Mexico, 1313 Goddard SE, Albuquerque, New Mexico 87106, USA

<sup>a)</sup> Author to whom correspondence should be addressed: [pierre.didier@telecom-paris.fr](mailto:pierre.didier@telecom-paris.fr)

## ABSTRACT

Interband cascade lasers are semiconductor lasers emitting in the mid-infrared domain but relying on interband transitions, contrary to their intersubband counterparts, quantum cascade lasers. Our experimental study of the relative intensity noise in a multi-mode interband cascade laser at  $4.1 \mu\text{m}$  shows that the room-temperature structure exhibits a relaxation frequency in the GHz range. We demonstrate that, far above the threshold current, the relaxation frequency increases with the bias current, and our simulations are in good agreement with our experimental efforts. Fitting of the relative intensity noise resonances gives access to several intrinsic parameters of the interband cascade laser under study such as differential gain, compression gain, and  $K$ -factor. This study is a clear step for understanding dynamics interplays in interband cascade laser structures, which means understanding the non-linear and modulation bandwidth limitations of such lasers.

Published under an exclusive license by AIP Publishing. <https://doi.org/10.1063/5.0070981>

The development of reliable, versatile, and efficient sources in the mid-infrared domain has become a key requirement for many applications. Supercontinuum generation in fibers or bulk crystals,<sup>1–3</sup> as well as optical parametric oscillators (OPOs),<sup>4</sup> are among the options. A main focus has been dedicated to semiconductor heterostructures generating mid-infrared light. Those are called cascade lasers, and the first technology that was introduced relied on intersubband transitions.<sup>5</sup> The resulting quantum cascade lasers (QCLs) were proven powerful for many applications such as spectroscopy of greenhouse gas molecules<sup>6</sup> or free-space communications in the transparency windows of the atmosphere.<sup>7</sup> The second technology was introduced by Yang in 1995<sup>8</sup> and is called interband cascade lasers (ICLs). The process relies on cascaded interband recombination in successive quantum wells, which limits the emission wavelength below  $7 \mu\text{m}$  at room temperature.<sup>9</sup> The ICL technology has been recently improved by replacing a single type-II interface by a W-shape configuration,<sup>10</sup> where an electron-hole is positioned between two electrons in the quantum well configuration. The consequence is a high electron-hole overlap despite the type-II alignment. Because they are interband lasers, ICLs exhibit carrier lifetime on the order of nanoseconds<sup>11</sup> that strongly exceeds typical photon lifetime of few picoseconds. This is a clear advantage compared to QCLs with picosecond carrier lifetime,<sup>12</sup> because this

means that ICL's performances are not hindered by phonon scattering losses. This property, combined with the W-shape configuration, decreases the current threshold density by one order of magnitude, leading to typical electrical power consumption below 1 W at peak optical power. This paves the way for light and portable systems with battery-driven ICLs. Integration of this mid-infrared technology can be further developed with ICLs on a silicon substrate for on-chip sensing technologies.<sup>13</sup> Application of ICLs has been extended to picosecond pulses<sup>14</sup> and free-space communication between 3 and  $5 \mu\text{m}$ , where the atmosphere is highly transparent. The maximum data rate one can expect with direct electrical modulation of an ICL is bounded by the laser's relaxation oscillation frequency. On the one hand, pioneer experimental efforts showed a modulation bandwidth of more than 3 GHz in a cryogenic ICL,<sup>15</sup> but subsequent efforts only achieved a maximum transmission rate of 70 Mb/s.<sup>16</sup> Recent free-space communication experiments have demonstrated hundreds of Mb/s data rates at room temperature,<sup>17,18</sup> while ICLs on RF-optimized mounts showed bandwidth in the GHz range at room temperature.<sup>19</sup> On the other hand, ICLs were found to exhibit multi-GHz non-linear dynamics bandwidth, both experimentally<sup>20</sup> and numerically,<sup>21</sup> which clearly advocates for a wide use in mid-infrared private communications.<sup>22</sup> Despite a clear development of experimental applications using ICLs,

the theory about their intrinsic properties is still scarce<sup>23,24</sup> and needs further investigation. A recent experimental analysis<sup>25</sup> has investigated the differential gain and gain compression factor of an ICL, but the conclusions are not compatible with the aforementioned literature describing high-speed capabilities. Furthermore, this effort did not succeed in observing ICL relaxation oscillations that we clearly exhibit in our experimental findings described hereinafter.

In this work, we numerically and experimentally study the relative intensity noise (RIN) of a Fabry-Pérot (FP) ICL to extract the relaxation frequency and subsequent key parameters such as differential gain, compression gain, and  $K$ -factor. The resonance is clearly seen in the RIN curves, and its frequency value increases when increasing the bias current of the ICL, as also expected from the theoretical viewpoint while previous experimental efforts about RIN in ICLs could not clearly exhibit the relaxation oscillation frequency. This work is of utter interest for the characterization of these novel mid-infrared semiconductor structures and will foster the development of further high-speed applications.

The  $4.1\ \mu\text{m}$  FP ICL under study is designed and manufactured at Université de Montpellier, and the details about the laser can be found in Fig. 1(a). The structure is grown by molecular beam epitaxy on a GaSb substrate. The active region is composed of seven-stage cascade periods of GaInSb type-II “W” quantum wells (QWs). This “W” design is a key tool for efficient interband recombination and is optimized for  $4.1\ \mu\text{m}$  lasing operation at room temperature. The process relies on interband recombination between the electron-hole and the

electron in the “W” QWs. Those are surrounded by an electron injector and an electron-hole injector. Electrons and holes are spread to the next cascade level thanks to quantum engineering of the band energy alignment and of the tunneling transitions. The active region is surrounded by the GaSb optical confinement layer and cladding with AlSb/InAs superlattices. The ICL was then soldered with indium on a copper block and mounted in a package with a direct connection between the SMA central contact and the laser ridge. A SMA-PCB end launch connector (Radiall R125539000) with a bandwidth of 18 GHz was used for this purpose. This is suitable for radio frequency modulation. The ICL is kept at a constant room temperature, and a continuous bias is provided by a low-noise current source (LDX-3232 CW QCL driver). The parameters of operation are described in Fig. 1(b), and the ICL has a threshold current of 75 mA at 297 K and a maximum beam power of 15 mW per facet at 185 mA and 4.3 V. This results in a wall-plug efficiency of 4%. As we carry out experiments with a multimode laser, as shown in the inset of Fig. 1(b), we can evaluate the mode spacing and obtain an average material index of  $n_g = 3.5$ .

In order to determine the bandwidth of the ICL, we performed optical and electrical rectifications, and later on, these bandwidths are compared with the extracted relaxation frequency. The rectification method<sup>26</sup> allows retrieving the electrical bandwidth without an optical detector, and it is, thus, widely used in the mid-infrared domain, where cheap room-temperature fast detectors are still missing.<sup>27</sup> We also evaluate the optical bandwidth by modulating the bias current with a sine wave and measuring the response with a 700 MHz bandwidth

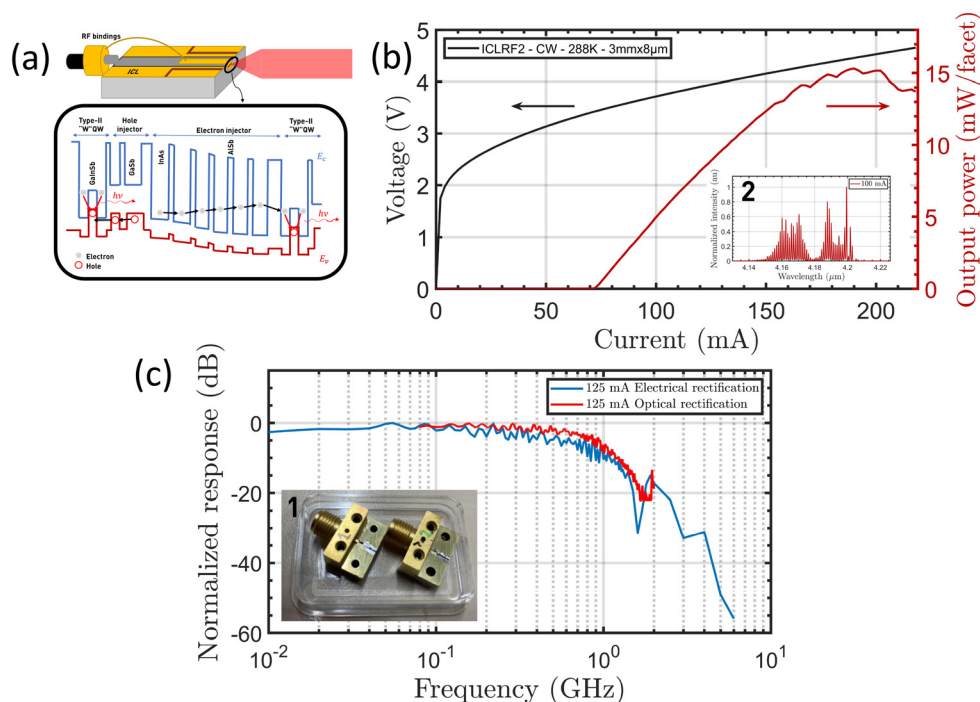


**FIG. 1.** (a) Schematic representation and simplified band diagram of our interband cascade laser at  $4.1\ \mu\text{m}$ . (b) ICL Light-intensity-voltage (PIV) curve under continuous wave pumping and a temperature of 288 K with typical optical spectrum in the inset. (c) The optical rectification is shown in red, and the electrical rectification is shown in blue for a supply current of 125 mA and a temperature of 288 K. The cutoff frequency is similar in both cases. The bottom left inset shows two ICLs mounted on a support suitable for high-frequency modulation.

mid-infrared detector. The electrical and optical rectification responses of the ICL are displayed in Fig. 1(c). The two 3 dB-bandwidths are consistent and are approximately 700 MHz at 288 K. In addition, the correlation between the electrical and optical bandwidths means that the mount of the ICL [inset of Fig. 1(c)] does not limit the modulation frequency. However, we do not see any clear indication of relaxation oscillations with these two methods.

Spontaneous noise is the main source of noise for optical sources, because it induces a variation of the optical output power. Moreover, circumventing noise limitations is of paramount importance in order to improve the quality of a laser transmission.<sup>28</sup> Because they are inter-band semiconductor lasers, ICLs are expected to operate in the class B regime with the upperstate lifetime often being much longer than the cavity damping time and that conveys a relaxation oscillation.<sup>29</sup> The RIN is the ratio between the power spectral density of the intensity noise and the squared average optical power.

In our configuration, depicted in Fig. 2, the ICL is biased with a low-noise current source and kept at room temperature. The optical signal generated by the ICL is collimated by a lens to a mercury-cadmium-telluride detector (MCT-VIGO UHSM-10.6) with a 3 dB-bandwidth of 1.3 GHz and 50  $\Omega$  loadout resistance. The 50  $\times$  50  $\mu\text{m}^2$  active area of this detector allows detecting mid-infrared signals down to a few hundreds of  $\mu\text{W}$ . The resulting electrical signal can be accessed via two SMA ports: a DC port for frequencies up to 300 Hz and an AC port for frequencies from 10 kHz. On the one hand, AC signal is amplified with a low-noise amplifier with 25-dB gain and 25-GHz bandwidth (SHF-826H) prior to the analysis with a 43-GHz bandwidth electrical spectrum analyzer (ESA-FSU Rohde&Schwarz). The RF power retrieved with the electrical spectrum analyzer is the difference between the noise contribution for the whole setup and the contribution for the setup without laser illumination. This corresponds to the first term in Eq. (1). On the other hand, the DC signal directly gives the evaluation of the shot noise of the detector, which corresponds to the second term in the following equation:

$$RIN(f) = \frac{S_p(f)}{BGR * I_{ph}^2} - \frac{2eB}{\langle I_{ph} \rangle}, \quad (1)$$

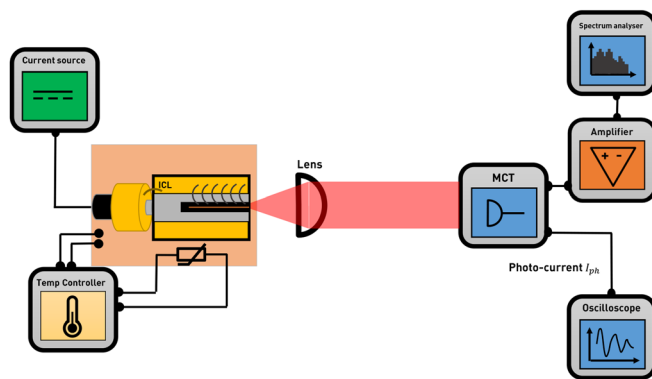


**FIG. 2.** Experimental setup for the determination of the RIN. The ICL is maintained at room temperature, and the distance between the emitting facet and the MCT detector is roughly 20 cm. Further analysis of the RIN signal leads to the determination of the relaxation frequency around the GHz.

where  $S_p(f) = S(f) - S_{dark}(f)$  with  $S_{dark}$  being the total noise caused by the setup without illumination, which will be considered as white noise,  $B$  being the resolution bandwidth of the ESA,  $G$  being the gain of the amplifier,  $R$  being the resistance of the detector,  $e$  being the electric charge carried by an electron, and  $I_{ph}$  being the photovoltaic current of the detector.

The study of the intensity noise allows determining the relaxation oscillation frequency as well as several intrinsic parameters of the laser structure, which is of paramount importance for nonlinear and high-speed applications. Previous studies showed a RIN around  $-130$  to  $-150$  dB/Hz (Refs. 23 and 24) but, because of a narrow detector bandwidth (400 MHz), did not exhibit any clear relaxation oscillation frequency. The RIN analysis for a wide frequency range is represented in Fig. 3(a). We show the evolution of the RIN for five different currents above  $1.8 \times I_{th}$  and at a constant temperature of 295 K. At low frequencies, around 10 MHz-100 MHz, the RIN level is significantly high, in the range of  $-95$  dB/Hz, and drops when increasing the frequency. As the ICL under study is multimode, various contributions can impact the noise level at low frequencies such as technical, thermal, or partition noises.<sup>30</sup> Moreover, for the aforementioned frequency range, the RIN increases when increasing the bias current. The most probable cause is the appearance of new modes in the optical spectrum leading to an increase in partition noise. Around 100-500 MHz, the impact of these phenomena diminishes, and the trend is reversed. The RIN decreases when the bias current is increased, which is in agreement with prior results.<sup>23,24</sup> By further increasing the frequency of the analysis, the relaxation oscillation of the ICL is clearly observed in the GHz range. Notably, the value of the relaxation frequency is large enough to achieve multi-Gbits/s data transmission and to expect a very large chaos bandwidth ( $>$ GHz), which is relevant for private optical communications. In addition, this result is of prime interest, because previous studies stated that the relaxation oscillation was above 3.2 GHz,<sup>15</sup> but that was not clearly unveiled in subsequent research works. As expected, Fig. 3(a) shows that the oscillation frequency increases with bias current. The relaxation oscillation was not observed for pump currents below  $1.52 \times I_{th}$  because of other substantial noise contributions and large damping factors. Finally, it is important to note that the noise is not influenced by the bias current after the relaxation oscillation. We estimate the shot noise of our detector to be around  $-135$  dB/Hz.

In order to access ICL's intrinsic parameters from the relaxation oscillations, a small signal analysis can be applied to the ICL's rate equations.<sup>24</sup> From this, an expression of the RIN can be retrieved and expressed as a function of angular frequency  $\omega$ ,

$$RIN(\omega) = \frac{a_1 + a_2 \omega^2}{S^2 \omega_R^4} |H(\omega)|^2, \quad (2)$$

where  $\omega_R$  is the angular relaxation frequency,  $S$  is the total photon number,  $a_1$  and  $a_2$  depend on intrinsic parameters of the ICL, and  $H$  is the modulation transfer function of the ICL taking into account the damping factor  $\gamma$  such as

$$H(\omega) = \frac{\omega_R^2}{\omega_R^2 - \omega^2 + j\omega\gamma}. \quad (3)$$

With the aforementioned model and the parameters that characterize the ICL under study, numerical simulation of the RIN is carried

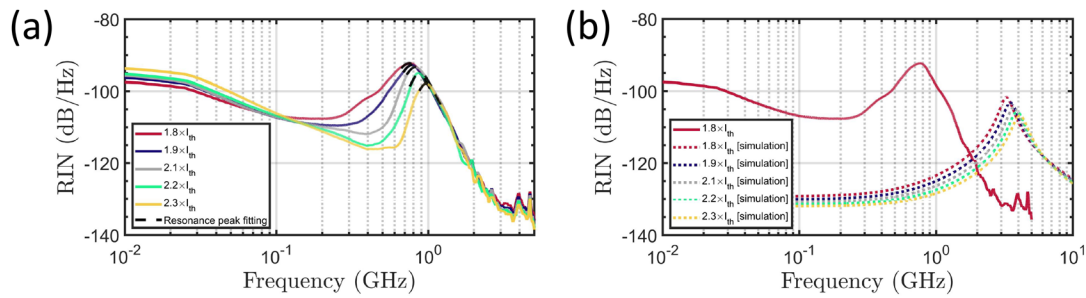


**FIG. 3.** (a) Relative intensity noise of the ICL at 295 K for various bias currents from  $1.8 \times I_{th}$  to  $2.3 \times I_{th}$ . Dashed black lines correspond to the fitting of the resonance associated with the relaxation oscillation. It leads to the determination of the relaxation frequency around the GHz. (b) Simulations of the intensity noise behavior for the laser under study, which shows good agreement with the experiment for 295 K and bias currents around  $2 \times I_{th}$ . The numerical model follows the work of Ref. 24, and relevant data used in the simulation are gathered in Table I.

out. Relevant parameters for the rate equations and, therefore, for RIN simulation are all gathered in Table I. Among them, only the injection current efficiency  $\eta$  and the spontaneous emission factor  $\beta$  were not directly accessible for the ICL under study. Typical values from the literature are chosen, that is to say,  $\eta = 34\%$  (Refs. 24 and 31) and  $\beta = 0.001$ .<sup>32</sup> As shown in Fig. 3(b), the evolution of the maximum of the resonance with the bias current is found in a good agreement with the experimental findings. However, it is relevant to note that the simulated RIN level is lower before relaxation oscillation, which is essentially attributed to the parasitic noise not taken into account in the simulation. Despite the fact that the shape of the relaxation oscillation is very similar, the related frequency is higher than the experimental one. Such a difference may be due to approximations made on intrinsic parameters, such as spontaneous emission factor, refractive index, optical confinement factor, and current injection efficiency, which are not easily accessible for ICLs. The two previous equations, (2) and (3), allow fitting the experimental RIN curves with a least squares approximation (dashed black curves in Fig. 3(a)). Those fittings are useful to determine the intrinsic parameters, such as angular relaxation frequency  $\omega_R$  and  $\gamma$ , as demonstrated hereafter. Theoretically, the squared frequency linearly evolves with the current offset<sup>29</sup> as follows:

$$f_R^2 = \frac{\Gamma_p \nu_g a}{4\pi^2 e V} \eta_i (I - I_{th}), \quad (4)$$

where  $\Gamma_p$  is the optical confinement factor,  $\nu_g$  is the group velocity in the active area,  $a$  is the differential gain,  $e$  is the charge of an electron,  $\eta_i$  is the injection efficiency, and  $V$  is the volume of the active area, whereas  $I$  and  $I_{th}$  are the bias current and the threshold current of the laser, respectively. In Fig. 4, the evolution of the squared resonance frequency is plotted as a function of the current offset  $I - I_{th}$ , associated with a linear fit at 293 K. From the slope of this curve, one can obtain the value of the differential gain in the ICL following Eq. (3). The differential gain  $a = \frac{dg}{dN}$  corresponds to the derivative of small signal gain with respect to the carrier density. When combined with a small active region, a large differential gain is a key material parameter for improving the laser's high-speed capabilities. From this work, the differential gain is estimated to be  $6 \times 10^{-17} \text{ cm}^2$  at 293 K, which is consistent with typical values already reported in QW lasers (for instance,  $a = 1.2 \times 10^{-16} \text{ cm}^2$  in Ref. 33).

Another parameter of interest for laser high-speed operation is the  $K$ -factor, which is a marker of the damping response. Large  $K$  prevents high-speed modulation, but in some cases, appropriate damping suppresses overshoot due to relaxation oscillations. The  $K$ -factor is defined as<sup>29</sup>

$$\gamma = Kf_R^2 + \gamma_0, \quad (5)$$

where  $f_R$  represents the relaxation oscillation frequency and  $\gamma_0$ , the damping offset, which is inversely proportional to the carrier lifetime.

**TABLE I.** List of ICL's parameters that are implemented in numerical simulations and in the fitting of the RIN.

Parameter	Value	Parameter	Value
Cavity length $L$	3 mm <sup>a</sup>	Photon lifetime $\tau_p$	7.6 ps <sup>a</sup>
Cavity width $W$	10 $\mu\text{m}$ <sup>a</sup>	Spontaneous emission time $\tau_{sp}$	15 ns <sup>a</sup>
Facet reflectivity $R$	0.32 <sup>a</sup>	Auger lifetime $\tau_{aug}$	1.08 ns <sup>a</sup>
Refractive index $n_r$	3.5 <sup>a</sup>	Differential gain $a$	$6 \times 10^{-17} \text{ cm}^2$ , <sup>b</sup>
Optical confinement factor $\Gamma_p$	0.23 <sup>a</sup>	Transparent carrier number $N_{tr}$	$10^{8,a}$
Internal loss $\alpha_i$	5 $\text{cm}^{-1,c}$	Spontaneous emission factor $\beta$	$10^{-3,d}$
Stage number $m$	7 <sup>a</sup>	Current injection efficiency $\eta$	0.34 <sup>a</sup>

<sup>a</sup>ICL data.

<sup>b</sup>Evaluated from fitting.

<sup>c</sup>Extrapolated from a similar structure emitting at  $3.3 \mu\text{m}$  (Refs. 31 and 34).

<sup>d</sup>ICL data from the literature.

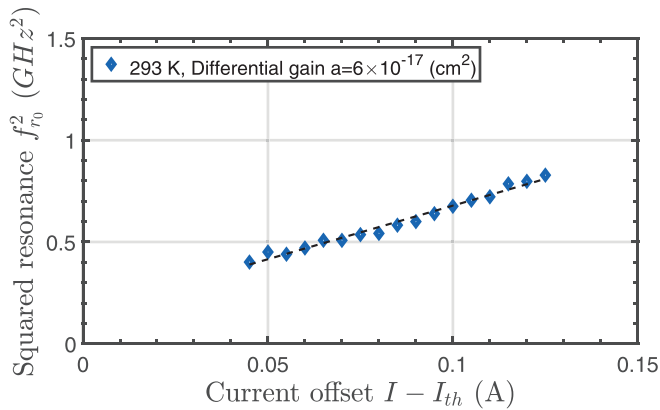


**FIG. 4.** Evolution of the squared resonance frequency as a function of the current offset  $I - I_{th}$ . The blue markers are the data points that are fitted using a regression line (dashed line).

In Fig. 5, the damping factor is plotted as a function of the squared resonance frequency at 293 K. From the linear fit,  $K = 3.7$  ns, which gives a maximum modulation bandwidth of 2.4 GHz according to the formula  $2\sqrt{2}\pi/K$ .<sup>24</sup> This result shows that ICLs are not limited to low-frequency operation<sup>25</sup> and can be deployed for multi-Gbits/s optical communication.<sup>18</sup> The damping factor offset  $\gamma_0 = 1.5$  ns<sup>-1</sup> leads to an effective carrier lifetime of 0.6 ns. Furthermore, we can also derive the gain compression factor  $\epsilon$ . This parameter may be used to describe the reduction in the optical gain above the threshold due to any other process such as spatial hole burning and carrier heating. In order to retrieve the gain compression factor, the following relationship can be used:

$$K = 4 * \pi^2 \left( \frac{\epsilon}{\nu_{ga}} + \tau_p \right). \quad (6)$$

The compression gain also accounts for the capability of a laser to be modulated at large output power. Here, using the previous findings, a value of  $\epsilon = 4.7 \times 10^{-17}$  cm<sup>3</sup> is extracted at 293 K. This result is in

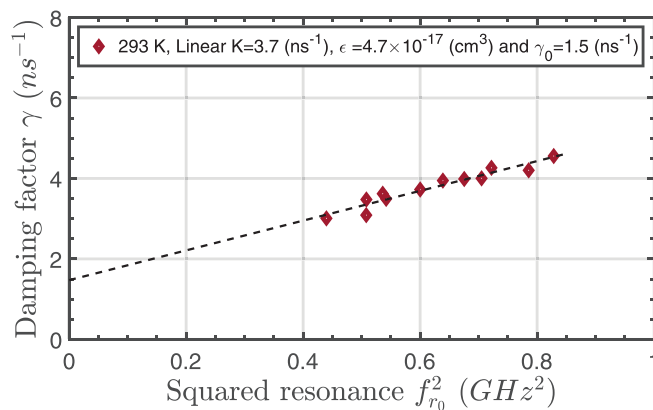


**FIG. 5.** Evolution of the damping factor as a function of the squared resonance at 293 K. The red markers are the data point, and the dashed line corresponds to the linear fit.

good agreement with a prior work about interband lasers, where a compression factor  $\epsilon = 1 \times 10^{-17}$  cm<sup>3</sup> was exhibited.<sup>35</sup> On top of that, it is relevant to highlight that the compression factor reported in this work is similar to that of QW lasers.

This paper reports on the intensity noise and intrinsic properties of a mid-infrared interband cascade laser emitting at 4.1  $\mu$ m. The results describe the unprecedented exhibition of the relaxation frequency in the GHz range, which is of first importance for enhancing modulation capabilities of such lasers. For that purpose, differential gain,  $K$ -factor, gain compression, and carrier lifetime are also analyzed. All these values are found consistent with those reported in interband quantum well lasers. The trends given by the simulations are also in good agreement with our experimental results. Differences between the experiment and the numerical simulation can be explained by the fact that the model did not take into account other types of noise, like spatial hole burning, thermal, and other parasitic noise. Further efforts will focus on developing a model that includes these phenomena. Overall, this work is a key step to consider ICLs for versatile, light, and cheap multi-Gbits/s transmission systems in the mid-infrared domain. In addition, these results confirm the potential of ICLs for broadband chaos, which is found useful in applications such as private optical communication and physical random bit generation. Optical injection and self-feedback are expected to improve the modulation bandwidth of this novel semiconductor laser, and this will be investigated in future experiments. The latter will also explore methods to reduce the RIN level with a view toward squeezed states of light in ICLs and shot-noise-limited mid-infrared sources. Such achievement could be a game changer in many applications, where ultra-low laser noise below the standard quantum limit is required like precision measurement, metrology, spectroscopy, and continuous-variable systems.

This work was supported by the French Defense Agency (DGA), the French ANR program (Nos. ANR-17-ASMA0006 and ANR-11-EQPX-0016), and the European Office of Aerospace Research and Development (No. FA9550-18-1-7001). The authors thank Professor Carlo Sirtori (ENS Paris) for lending the MCT detector used in this experiment.

## AUTHOR DECLARATIONS

### Conflict of Interest

The authors have no conflicts of interest to disclose.

### DATA AVAILABILITY

The data that support the findings of this study are available from the corresponding author upon reasonable request.

## REFERENCES

- J. H. Price, T. M. Monro, H. Ebendorff-Heidepriem, F. Poletti, P. Horak, V. Finazzi, J. Y. Leong, P. Petropoulos, J. C. Flanagan, G. Brambilla *et al.*, "Mid-IR supercontinuum generation from nonsilica microstructured optical fibers," *IEEE J. Sel. Top. Quantum Electron.* **13**, 738–749 (2007).
- P. Domachuk, N. Wolchover, M. Cronin-Golomb, A. Wang, A. K. George, C. Cordeiro, J. C. Knight, and F. Omenetto, "Over 4000 nm bandwidth of mid-IR supercontinuum generation in sub-centimeter segments of highly nonlinear tellurite PCFs," *Opt. Express* **16**, 7161–7168 (2008).
- F. Silva, D. Austin, A. Thai, M. Baudisch, M. Hemmer, D. Faccio, A. Couairon, and J. Biegert, "Multi-octave supercontinuum generation from mid-infrared filamentation in a bulk crystal," *Nat. Commun.* **3**(1), 807 (2012).

- <sup>4</sup>B. Cole, L. Goldberg, S. Chinn, L. A. Pomeranz, K. T. Zawilski, P. G. Schunemann, and J. McCarthy, "Compact and efficient mid-IR OPO source pumped by a passively Q-switched Tm: YAP laser," *Opt. Lett.* **43**, 1099–1102 (2018).
- <sup>5</sup>J. Faist, F. Capasso, D. L. Sivco, C. Sirtori, A. L. Hutchinson, and A. Y. Cho, "Quantum cascade laser," *Science* **264**, 553–556 (1994).
- <sup>6</sup>G. Santoni, B. C. Daube, E. Kort, R. Jiménez, S. Park, J. Pittman, E. Gottlieb, B. Xiang, M. Zahniser, D. Nelson *et al.*, "Evaluation of the airborne quantum cascade laser spectrometer (QCLS) measurements of the carbon and greenhouse gas suite—CO<sub>2</sub>, CH<sub>4</sub>, N<sub>2</sub>O, and CO—during the CalNex and HIPPO campaigns," *Atmos. Meas. Tech.* **7**, 1509–1526 (2014).
- <sup>7</sup>S. Blaser, D. Hofstetter, M. Beck, and J. Faist, "Free-space optical data link using Peltier-cooled quantum cascade laser," *Electron. Lett.* **37**, 778–780 (2001).
- <sup>8</sup>R. Q. Yang, "Infrared laser based on intersubband transitions in quantum wells," *Superlattices Microstruct.* **17**, 77–83 (1995).
- <sup>9</sup>R. Q. Yang, L. Li, W. Huang, S. M. S. Rassel, J. A. Gupta, A. Bezinger, X. Wu, S. G. Razavipour, and G. C. Aers, "InAs-based interband cascade lasers," *IEEE J. Sel. Top. Quantum Electron.* **25**(6), 1200108 (2019).
- <sup>10</sup>J. Meyer, C. Hoffman, F. Bartoli, and L. Ram-Mohan, "Type-II quantum-well lasers for the mid-wavelength infrared," *Appl. Phys. Lett.* **67**, 757–759 (1995).
- <sup>11</sup>W. Bewley, J. Lindle, C. Kim, M. Kim, C. Canedy, I. Vurgaftman, and J. Meyer, "Lifetimes and Auger coefficients in type-II W interband cascade lasers," *Appl. Phys. Lett.* **93**, 041118 (2008).
- <sup>12</sup>G. Paulavičius, V. Mitin, and M. Strosio, "Hot-optical-phonon effects on electron relaxation in an AlGaAs/GaAs quantum cascade laser structure," *J. Appl. Phys.* **84**, 3459–3466 (1998).
- <sup>13</sup>A. Spott, E. J. Stanton, A. Torres, M. L. Davenport, C. L. Canedy, I. Vurgaftman, M. Kim, C. S. Kim, C. D. Merritt, W. W. Bewley *et al.*, "Interband cascade laser on silicon," *Optica* **5**, 996–1005 (2018).
- <sup>14</sup>J. Hillbrand, M. Beiser, A. M. Andrews, H. Detz, R. Weih, A. Schade, S. Höfling, G. Strasser, and B. Schwarz, "Picosecond pulses from a mid-infrared interband cascade laser," *Optica* **6**, 1334–1337 (2019).
- <sup>15</sup>A. Soibel, M. Wright, W. Farr, S. Keo, C. Hill, R. Q. Yang, and H. Liu, "High-speed operation of interband cascade lasers," *Electron. Lett.* **45**, 264–265 (2009).
- <sup>16</sup>A. Soibel, M. W. Wright, W. H. Farr, S. A. Keo, C. J. Hill, R. Q. Yang, and H. Liu, "Midinfrared interband cascade laser for free space optical communication," *IEEE Photonics Technol. Lett.* **22**, 121–123 (2010).
- <sup>17</sup>J. Mikołajczyk, R. Weih, and M. Motyka, "Optical wireless link operated at the wavelength of 4.0  $\mu\text{m}$  with commercially available interband cascade laser," *Sensors* **21**, 4102 (2021).
- <sup>18</sup>O. Spitz, P. Didier, L. Durupt, D. A. Díaz-Thomas, A. N. Baranov, L. Cerutti, and F. Grillot, "Free-space communication with directly modulated mid-infrared quantum cascade devices," *IEEE J. Sel. Top. Quantum Electron.* **28**, 1–9 (2022).
- <sup>19</sup>H. Lotfi, L. Li, L. Lei, H. Ye, S. Shazzad Rassel, Y. Jiang, R. Q. Yang, T. D. Mishima, M. B. Santos, J. A. Gupta *et al.*, "High-frequency operation of a mid-infrared interband cascade system at room temperature," *Appl. Phys. Lett.* **108**, 201101 (2016).
- <sup>20</sup>O. Spitz, J. Wu, P. Didier, D. Díaz-Thomas, L. Cerutti, A. Baranov, G. Maisons, M. Carras, C.-W. Wong, and F. Grillot, "Chaos bandwidth in mid-infrared quantum cascade photonic devices with interband and intersubband transitions," in *CLEO: Science and Innovations* (Optical Society of America, 2021), p. STu1H-4.
- <sup>21</sup>H. Han, X. Cheng, Z. Jia, and K. A. Shore, "Nonlinear dynamics of interband cascade laser subjected to optical feedback," *Photonics* **8**, 366 (2021).
- <sup>22</sup>O. Spitz, A. Herdt, J. Wu, G. Maisons, M. Carras, C.-W. Wong, W. Elsässer, and F. Grillot, "Private communication with quantum cascade laser photonic chaos," *Nat. Commun.* **12**, 3327 (2021).
- <sup>23</sup>P. A. Folkes, "Interband cascade laser photon noise," *J. Phys. D: Appl. Phys.* **41**, 245109 (2008).
- <sup>24</sup>Y. Deng, B.-B. Zhao, Y.-T. Gu, and C. Wang, "Relative intensity noise of a continuous-wave interband cascade laser at room temperature," *Opt. Lett.* **44**, 1375–1378 (2019).
- <sup>25</sup>Z.-F. Fan, Y. Deng, C. Ning, S.-M. Liu, and C. Wang, "Differential gain and gain compression of an overdamped interband cascade laser," *Appl. Phys. Lett.* **119**, 081101 (2021).
- <sup>26</sup>H. Liu, J. Li, M. Buchanan, and Z. Wasilewski, "High-frequency quantum-well infrared photodetectors measured by microwave-rectification technique," *IEEE J. Quantum Electron.* **32**, 1024–1028 (1996).
- <sup>27</sup>K. Yang, J. Liu, S. Zhai, J. Zhang, N. Zhuo, L. Wang, S. Liu, and F. Liu, "Room-temperature quantum cascade laser packaged module at 8  $\mu\text{m}$  designed for high-frequency response," *Electron. Lett.* **57**, 665–667 (2021).
- <sup>28</sup>X. Pang, O. Ozolins, L. Zhang, R. Schatz, A. Udalcovs, J. Storck, G. Maisons, M. Carras, S. Xiao, G. Jacobsen *et al.*, "4 Gbps PAM-4 and DMT free space transmission using a 4.65  $\mu\text{m}$  quantum cascade laser at room temperature," in *2017 European Conference on Optical Communication (ECOC)* (IEEE, 2017), pp. 1–3.
- <sup>29</sup>L. A. Coldren, S. W. Corzine, and M. L. Mashanovitch, *Diode Lasers and Photonic Integrated Circuits* (John Wiley & Sons, 2012), Vol. 218.
- <sup>30</sup>K. Petermann, *Laser Diode Modulation and Noise* (Springer Science & Business Media, 1991), Vol. 3.
- <sup>31</sup>D. A. Díaz-Thomas, "Design, fabrication and investigation of Interband Cascade structures for mid-IR VCSELs," Ph.D. thesis (Université de Montpellier, 2020).
- <sup>32</sup>D. Ding, S. R. Johnson, J.-B. Wang, S.-Q. Yu, and Y.-H. Zhang, "Determination of spontaneous emission quantum efficiency in InGaAs/GaAs quantum well structures," *Proc. SPIE* **6841**, 68410D (2008).
- <sup>33</sup>M. Tatham, I. Lealman, C. P. Seltzer, L. Westbrook, and D. Cooper, "Resonance frequency, damping, and differential gain in 1.5  $\mu\text{m}$  multiple quantum-well lasers," *IEEE J. Quantum Electron.* **28**, 408–414 (1992).
- <sup>34</sup>J. R. Meyer, W. W. Bewley, C. L. Canedy, C. S. Kim, M. Kim, C. D. Merritt, and I. Vurgaftman, *The Interband Cascade Laser* (Multidisciplinary Digital Publishing Institute, 2020), p. 75.
- <sup>35</sup>R. Nagarajan, T. Fukushima, M. Ishikawa, J. E. Bowers, R. S. Geels, and L. A. Coldren, "Transport limits in high-speed quantum-well lasers: Experiment and theory," *IEEE Photonics Technol. Lett.* **4**, 121–123 (1992).